Bubble-free and pulse-free fluid delivery into microfluidic devices

Yang Jun Kang,[1,2] Eunseop Yeom,[2] Eunseok Seo,[3] and Sang-Joon Lee[1,2,a)]
[1]*Center for Biofluid and Biomimic Research, Pohang University of Science and Technology, Pohang, South Korea*
[2]*Department of Mechanical Engineering, Pohang University of Science and Technology, Pohang, South Korea*
[3]*Division of Integrative Biosciences and Biotechnology, Pohang University of Science and Technology, Pohang, South Korea*

(Received 23 December 2013; accepted 15 January 2014; published online 29 January 2014)

The bubble-free and pulse-free fluid delivery is critical to reliable operation of microfluidic devices. In this study, we propose a new method for stable bubble-free and pulse-free fluid delivery in a microfluidic device. Gas bubbles are separated from liquid by using the density difference between liquid and gas in a closed cavity. The pulsatile flow caused by a peristaltic pump is stabilized via gas compressibility. To demonstrate the proposed method, a fluidic chamber which is composed of two needles for inlet and outlet, one needle for a pinch valve and a closed cavity is carefully designed. By manipulating the opening or closing of the pinch valve, fluids fill up the fluidic chamber or are delivered into a microfluidic device through the fluidic chamber in a bubble-free and pulse-free manner. The performance of the proposed method in bubble-free and pulse-free fluid delivery is quantitatively evaluated. The proposed method is then applied to monitor the temporal variations of fluidic flows of rat blood circulating within a complex fluidic network including a rat, a pinch valve, a reservoir, a peristaltic pump, and the microfluidic device. In addition, the deformability of red blood cells and platelet aggregation are quantitatively evaluated from the information on the temporal variations of blood flows in the microfluidic device. These experimental demonstrations confirm that the proposed method is a promising tool for stable, bubble-free, and pulse-free supply of fluids, including whole blood, into a microfluidic device. Furthermore, the proposed method will be used to quantify the biophysical properties of blood circulating within an extracorporeal bypass loop of animal models. © *2014 AIP Publishing LLC*. [http://dx.doi.org/10.1063/1.4863355]

I. INTRODUCTION

Microfluidic devices, which have distinctive advantages over conventional methods, have been successfully demonstrated for various applications in drug delivery,[1–5] accurate dispensing,[6] analytical devices,[7–9] clinical diagnostics,[10–13] point-of-care-testing,[14,15] and cell studies.[16–18] Based on fluid transport in microfluidic channels, the microfluidic devices can achieve their unique functions such as manipulation,[19–22] mixing,[23–25] and analysis.[26,27] However, these devices encounter several problems including clogging,[28,29] leakages,[30] unwanted bubble accumulations,[31] and unstable fluidic flows[32] in the course of determining the biophysical properties of cells.[33] Among these issues, bubble-free and pulse-free fluid delivery has been considered as essential for reliable operation of microfluidic devices. Air bubbles from several sources, including sample perfusion, tube connections, and variations in temperature and pressure, are occasionally introduced in a microfluidic device. Owing to surface tension of

a)Author to whom correspondence should be addressed. Electronic mail: sjlee@postech.ac.kr. Fax: +82-54-279-3199

liquid-air interface, air bubbles cause to distort or impede fluidic flows in the microfluidic channel and lead to serious cell damage. During the trapping and removal process of air bubbles, unstable liquid flows occur inside the microfluidic channels. In addition, a peristaltic pump, which is commonly used in microfluidic devices, induces unstable fluid delivery. These unstable liquid flows in the microfluidic channel, i.e., the inconsistent behaviour of test fluids, cause the microfluidic device to encounter some errors. Thus, to achieve satisfactory performance and consistent function of a microfluidic device, test fluid should be delivered in a bubble-free and pulse-free manner.

Previous studies have introduced several bubble-free techniques for cell cultures in a microfluidic device, because air bubbles are cytotoxic to cells and affect cell viability adversely. For example, ultrasonic-driven degassing,[34] buoyance of air bubbles,[31,35] bubble trap,[36–38] and porous membrane[39–42] have been used to avoid air bubble accumulation in microfluidic channels. Furthermore, an active bubble removal technique using an external vacuum pump was suggested to remove air bubbles completely within a short period (∼min).[37,38,41] However, loss of sample liquids occurs during active bubble removal using a vacuum pump. In addition, real-time monitoring of fluidic flows is required for the immediate removal of the air bubbles that abruptly appear in a microfluidic channel.

Although these methods have been successfully demonstrated in the trapping or removal of air bubbles, they still have technical limitations in ensuring consistent fluidic flows. That is, these bubble removal techniques cannot be considered as ideal solutions to ensure consistent fluidic flows in a microfluidic channel because small air bubbles disturb or impede liquid flows in the microfluidic channel during their removal. The performance of the microfluidic device is likely to deteriorate because of unstable fluid flows in the microfluidic channel. Therefore, a flow stabilization technique is essential to provide reliable fluidic flows in microfluidic devices.

Several methods, including flexible membranes in series[32] or parallel,[43] air compressibility,[44] and active membrane control,[45,46] have been suggested for consistent fluidic delivery into a microfluidic device. The compliance effect resulting from membrane deflection facilitates stabilization of the fluctuations in fluidic flows. Although these methods can deliver test fluids consistently, they do not take a part in avoiding delivery of air bubbles into a microfluidic channel. Therefore, for consistent delivery of liquids into a microfluidic device, air bubbles should be trapped or removed before entering into a microfluidic device. Simultaneously, flow disturbances and unstable fluctuations should be minimized during the trapping or removal of air bubbles.

In this study, we propose a new fluidic device for the bubble-free and pulse-free fluid delivery into microfluidic environments. The proposed method is based on bubble separation using density difference and flow stabilization using air compressibility. The proposed method can supply liquids into a microfluidic device in a bubble-free and pulse-free manner. Taking into account the fact that most previous methods were incapable of supplying fluids into a microfluidic device in a bubble-free and pulse-free manner, we believe that the proposed method has distinctive advantages because of its ability to deliver liquids into a microfluidic device consistently and reliably. First, the proposed approach can deliver test samples into a microfluidic device without air bubbles and noticeable pulses. Second, this method does not require flow control devices, such as pressure controller or a vacuum pump. The liquid loss incurred from vacuum pump operation can be avoided. Third, the proposed technique does not require the real-time monitoring of fluidic flows in a microfluidic channel. Finally, the proposed method can minimize the back flow induced by peristaltic pump operation in a microfluidic channel because the inlet is disconnected from the outlet. Thus, the proposed method facilitates the reliable and consistent performance of the microfluidic device.

The performance of the proposed method is quantitatively evaluated for the bubble-free and pulse-free delivery functions separately. After its feasibility and usefulness are verified, the proposed method is applied to monitor the temporal variations of the fluidic flows of rat blood circulating in a complex fluidic network, which includes a rat, a pinch valve, a reservoir, a peristaltic pump, and a microfluidic device. Lastly, the temporal variations of the blood flows are used to evaluate deformability of red blood cells (RBCs) and platelet aggregation in a microfluidic device.

II. PROPOSED FLUIDIC CHAMBER FOR BUBBLE-FREE AND PULSE-FREE FLUID DELIVERY

In this study, we propose a simple but effective fluidic chamber for bubble-free and pulse-free fluid delivery into a microfluidic environment. The proposed method simultaneously employs the density difference-based bubble separation for bubble-free delivery and the air compressibility-based flow stabilization technique for pulse-free delivery. Depending on density difference between liquid and gas, gas bubbles are partially segregated in a specific-sized cavity of the fluidic chamber. Liquid droplets fall down on the gas-liquid interface because of gravity effect. After penetrating into the liquid, the dissolved gas bubbles in the liquid droplet are completely separated by the buoyancy effect and then released to the gas layer. Meanwhile, unstable fluidic flows caused by a peristaltic pump or gas bubbles are sufficiently stabilized by employing the compliance effect that results from gas compressibility in the closed cavity. Thus, for reliable operation of the microfluidic device, the proposed method can supply test samples into a microfluidic device in a bubble-free and pulse-free manner.

To demonstrate the proposed method, a fluidic chamber, which is composed of two needles for inlet and outlet, one needle for a pinch valve and a specific-sized cavity, is carefully designed. By manipulating the pinch valve as the flow controller, test liquid fills up the fluidic cavity and is then supplied into the microfluidic device. To avoid liquid loss from the fluidic chamber, the pinch valve is positioned sufficiently above the inlet needle. In addition, because the inlet needle and outlet needle are disconnected vertically, the back flow caused by the peristaltic pump has a negligible influence on the fluid delivery into the microfluidic device.

As illustrated in Fig. 1**A**, the proposed fluidic chamber is connected to a complex fluidic network that includes a rat, a pinch valve, a reservoir, a peristaltic pump, and the microfluidic device. Rat blood flows from the femoral artery into a reservoir by adjusting the pinch valve. The rat blood within the reservoir is then supplied into the fluidic chamber using a peristaltic pump (MP-1000, Tokyo Rikakikai Co., Japan). During rat blood perfusion using the peristaltic pump, pulsatile and back flows occur. Oxygen bubbles are continuously generated because of the squeeze motion of RBCs in the peristaltic pump. Thus, rat blood and oxygen bubbles are sequentially supplied into the fluidic chamber. After passing through the inlet needle of the proposed fluidic chamber, gas bubbles are spread in the spacious cavity. A droplet including rat blood and oxygen bubbles is formed on the tip of the inlet needle. This droplet falls down on gas-liquid interface in the cavity. When the droplet penetrates into the blood preserved in the cavity, the oxygen bubbles are then separated into the gas phase. Thus, rat blood is delivered into the microfluidic device because oxygen bubbles are separated in the proposed fluidic chamber. In addition, unstable flow fluctuations, including pulsatile and back flows, are completely stabilized by the compliance effect resulting from oxygen-gas compressibility. Thereafter, rat blood is exclusively delivered into the microfluidic device in a bubble-free and pulse-free manner.

The transport of test fluid in the proposed fluidic chamber is controlled by the opening or closing of the pinch valve. To avoid the problem of serious gas bubble delivery into the microfluidic device, the cavity of the fluidic chamber is sufficiently filled with liquid by opening the pinch valve [Fig. 1**B**-a]. During this process, the liquid is not supplied into the microfluidic device because the pressure conditions at inlet and outlet of the microfluidic device are the same. Thus, the liquid volume in the cavity increases while gas leaks out through the pinch valve. The pinch valve is kept open until the cavity is filled with liquid up to a specific volume (V_{liquid}) [Fig. 1**B**-b]. After the pinch valve is closed, the liquid flows into the microfluidic device because of the pressure difference between the fluidic chamber and microfluidic device [Fig. 1**B**-c].

In the fluidic chamber, the droplet impact behavior on the gas-liquid interface and bubble separation is visualized by using a high-speed camera (FASTCAM SA1.1, Photron, USA). Fig. 1**C** shows sequential images illustrating the dynamic behavior of impact droplet and gas bubble separation with respect to time [(a) $t = 0$, (b) $t = 4$ ms, (c) $t = 6$ ms, (d) $t = 9$ ms, (e) $t = 15$ ms, (f) $t = 45$ ms, (g) $t = 210$ ms, and (h) $t = 290$ ms]. As expected, the gas bubbles are separated from the liquid and floated toward the gas-liquid interface.

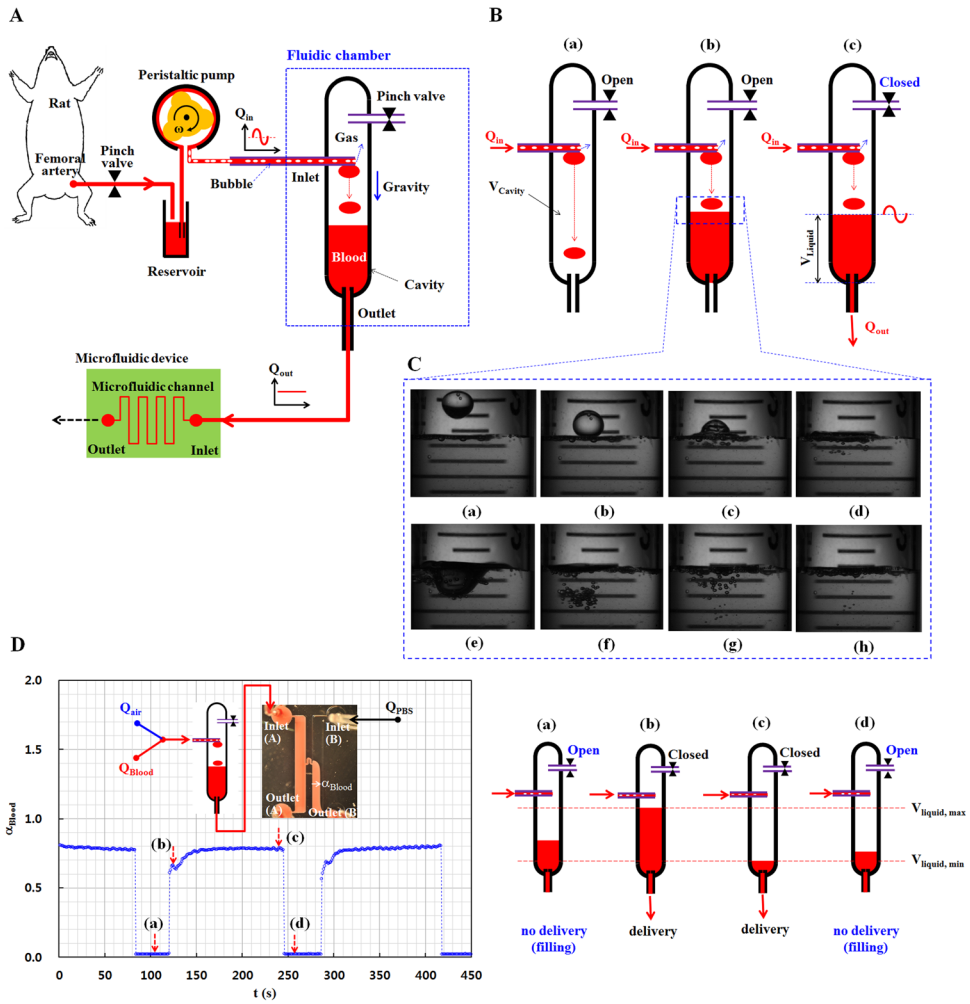

FIG. 1. Schematics of the proposed fluidic device for bubble-free and pulse-free fluid delivery into a microfluidic device. (**A**) The fluidic device is composed of two needles for the inlet and the outlet, one needle for the pinch valve and a specific-sized cavity. During the perfusion of rat blood, oxygen bubbles and pulsatile flows are caused by a peristaltic pump. Through the proposed fluidic device, oxygen bubbles are completely separated from rat blood. Thus, rat blood is consistently supplied into the microfluidic device. (**B**) By manipulating the pinch valve, rat blood fills up the cavity of the fluidic chamber or is delivered into the microfluidic device. (a) After the pinch valve is opened, the fluidic chamber is filled with rat blood. (b) The pinch valve remains open until the cavity is filled with rat blood, up to a volume of V_{liquid}. (c) Rat blood is supplied into the microfluidic device by closing the pinching valve. (**C**) Microscopic images captured consecutively with a high-speed camera show the separation of gas bubbles from a droplet of liquid with respect to time [(a) $t = 0$, (b) $t = 4$ ms, (c) $t = 6$ ms, (d) $t = 9$ ms, (e) $t = 15$ ms, (f) $t = 45$ ms, (g) $t = 210$ ms, and (h) $t = 290$ ms]. (**D**) Temporal variations of the blood-filled width (α_{Blood}) in the right-side channel, depending on the manipulation of the pinch valve [(a) "open" for filling up fluid, (b) to (c) "closed" for delivering fluid, and (d) "open" again for filling up fluid].

As a preliminary demonstration of the proposed method, a microfluidic network is established by connecting the proposed fluidic chamber to a microfluidic analogue of the Wheastone-bridge channel, as shown in the inset of Fig. 1**D**. For convenience, the cavity volume within the proposed fluidic chamber is designed to be 1 m*l* ($V_{cavity} = 1$ m*l*). To deliver the test fluid in gas-blood phase into the proposed fluidic chamber, blood (RBCs in phosphate buffered saline (PBS) suspension, $H_{ct} = 40\%$) is supplied at a flow rate of 2 m*l*/h ($Q_{Blood} = 2$ m*l*/h) using a syringe pump (neMESYS, Cetoni GmbH, Germany). Air bubbles are delivered by a peristaltic pump at the rotating speed of 3 ($\omega = 3$). The test fluid comprising blood with air bubbles is supplied into the proposed fluidic chamber. Because air bubbles are separated from the test fluid in fluidic chamber, blood is only delivered into the inlet (A) of the microfluidic device. To monitor the fluidic behavior of the test fluid in the microfluidic channel, 1× PBS

solution is supplied as reference fluid at the flow rate of $Q_{PBS} = 2$ m*l*/h into the inlet (B) of the microfluidic device using a syringe pump. Temporal variations of the interfacial position between test fluid and reference fluid (α_{Blood}) are quantitatively evaluated based on the microscopic images captured consecutively using a high speed camera (PCO, Germany).

Fig. 1**D** shows the periodic variations of the interfacial position (α_{Blood}) depending on the manipulation of the pinch valve. After the pinch valve is opened, the flow rate of blood is fixed as 50 m*l*/h, to fill up the cavity sufficiently within a short period. The fluidic chamber tends to be filled with test fluid and some air-bubbles are discharged [Fig. 1**D**-a]. According to flow-pattern analysis, the α_{Blood} remains constant. This result indicates that the test fluid is not supplied into the microfluidic device, despite the high flow rate. After the test fluid volume reaches approximately 0.6 m*l* ($V_{liquid,\ max} = 0.6$ m*l*) for 34 ± 2.84 s, the pinch valve is closed [Fig. 1**D**-b]. As expected, air bubbles are completely trapped, and only blood is supplied into the microfluidic device. In the proposed fluidic chamber, temporal variations of the interfacial position (α_{Blood}) are stable, after exhibiting transient behaviors owing to air compliance resulting from air compressibility. During the perfusion of test fluid, the blood volume is decreased, because air bubbles continuously enter into the fluidic chamber. Blood delivery is nearly consistent for 133 ± 2.8 s, until the blood volume is decreased to 0.1 m*l* ($V_{liquid,\ min} = 0.1$ m*l*) [Fig. 1**D**-c]. Taking into account the fact that air fills up 0.5 m*l* within the cavity for a specific delivery time period, the flow rate of the air supplied by the peristaltic pump is estimated to be 15.34 ± 0.43 m*l*/h. Thereafter, to prevent air bubbles into the microfluidic device, blood is filled up to $V_{liquid,\ max}$, at the flow rate of 50 m*l*/h, by opening the pinch valve [Fig. 1**D**-d].

This preliminary demonstration shows that the proposed fluidic chamber can prevent delivery of air bubbles into the microfluidic device, through proper manipulation of the pinch valve. In addition, blood is delivered into the microfluidic device consistently and stably.

III. MATERIALS AND METHODS

A. Fabrication of the proposed fluidic chamber and microfluidic device

A plunger rod in a syringe (1 m*l*) is carefully fixed to maintain a specific cavity volume (V_{cavity}). After the plastic cap of the steel needle (23 gauge) is removed, two needles for the inlet and pinch valve are inserted into the syringe tube as shown in Fig. 1**A**. Epoxy is used to fix the needles. A pinch valve is installed in the middle of a flexible tube (ID = 500 μm), which is connected to the needle for the pinch valve. The proposed fluidic chamber is prepared after two needles for inlet and outlet are connected to the flexible tubes.

A microfluidic device is designed to have two inlets (A and B) and outlets (A and B), two identical side channels (width = 1000 μm), and one bridge channel (width = 100 μm) connecting the two side channels. The channel depth is fixed at 50 μm. To prepare the microfluidic device based on a soft lithography process, a silicon molder is fabricated using MEMS technologies. After polydimethylsiloxane (PDMS) (Sylgard 184, Dow Corning, USA) is poured on the silicon molder and cured at 80 °C for 3 h, a PDMS block is peeled off from the silicon molder. After oxygen plasma treatment, the microfluidic device is prepared by bonding the PDMS block on the glass substrate.

B. Experimental setup and image processing

The microfluidic device is mounted on an optical microscope (Nikon, Tokyo, Japan) equipped with a charged coupled device (CCD) camera (PCO, Germany) or a stereo microscope (Stemi 2000-C, Zeiss, Germany) equipped with a digital camera (D700, Nikon, Japan). Using commercial software (Matlab, Mathworks, USA), temporal variations of the fluid flows in the microfluidic channel are quantitatively evaluated using microscopic images captured consecutively by the CCD camera or the digital camera. In this study, gray image or color image is converted into a binary image by adopting the Otsu's method. After determining the region of interest (ROI) for each image, fluid flows in the microfluidic channel are quantitatively analyzed with respect to time. Depending on experimental conditions, blood sample as test fluid is

supplied by using a peristaltic pump (MP-1000, Tokyo Rikakikai Co., Japan) or a syringe pump (neMESYS, Centoni Gmbh, Germany). In addition, PBS solution (pH 7.4, Bio Solution, Korea) is delivered as reference fluid using the syringe pump. All experiments are conducted at constant room temperature (25 °C).

C. Sample preparation

The human blood samples tested in this study were provided by a blood bank (Daegu-Kyeongbuk Blood Bank, Korea). The hematocrit of blood samples was adjusted to 40% by carefully adjusting the RBCs or PBS solution. To evaluate the temporal variations of blood flows attributed to deformability of RBCs, the membrane of RBCs is chemically fixed by maintaining RBCs in PBS solution containing concentrations of glutaraldehyde (GA) [(a) $C_{GA} = 0.13\%$, (b) $C_{GA} = 0.25\%$] at 25 °C for 10 min.

D. Preparation of rat model and extracorporeal rat-bypass loop

In this study, all experiments using animal models are conducted according to "the test guidelines on the use of laboratory animals" issued by the POSTECH Ethics Committee. A male Sprague–Dawley rat (14 weeks old, 0.362 kg body weight) is anesthetized with an intramuscular injection of ketamine (100 mg/kg) and xylazine (10 mg/kg). To prevent blood clotting in vascular vessels, heparin (1000 IU/m*l*/kg) is injected through the tail vein. After waiting for 10 min from the heparin injection, a left femoral artery is cannulated with one end of a polyethylene tube (ID = 580 μm) filled with heparin (10 IU/m*l*). The other end of the polyethylene tube is connected to a reservoir. A pinch valve is used to regulate the blood flow from the rat. The other polyethylene tube (ID = 500 μm) is used to connect the reservoir to the proposed fluidic device and the microfluidic device. After an extracorporeal rat-bypass loop is established, the rat blood in the reservoir is delivered into the microfluidic device using the peristaltic pump. At the end of each experiment, the rat model is sacrificed under an anesthetic state according to the "test guidelines of laboratory animals."

IV. RESULTS AND DISCUSSION

A. Bubble-free fluid delivery

To demonstrate the bubble-free delivery of the proposed fluidic chamber, human blood and air bubbles are simultaneously delivered into the proposed fluidic chamber. As shown in Fig. 2**A**-a, air bubbles are delivered into the inlet (A) of the microfluidic device by operating the peristaltic pump, at a pumping speed of 1.6 ($\omega = 1.6$). The blood sample is supplied into the inlet (B) of the microfluidic device, at a flow rate of 3 m*l*/h ($Q_{Blood} = 3$ m*l*/h) using the syringe pump. Because the outlet (A) was closed, air unexceptionally enters into the right-side channel. Blood and air bubbles are sequentially moved from the outlet (B) to the proposed fluidic chamber, as shown in Fig. 2**A**-b. According to the proposed method, air bubbles are separated from the blood sample completely. Therefore, blood is only delivered into the microfluidic device consistently. For this experimental demonstration, the cavity volume of the fluidic device is set to 0.5 m*l* ($V_{cavity} = 0.5$ m*l*). When the inlet (B) and the outlet (B) of the microfluidic device are closed as shown in Fig. 2**A**-c, blood flows only along the left- side channel.

To evaluate quantitatively the delivery of air bubbles into the microfluidic device from the proposed chamber, the area filled with blood (ϕ_{Blood}) in a ROI (460 × 600 pixels) is calculated from each microscopic image using commercial software. Fig. 2**B** shows temporal variations of the area filled with blood in the ROI when the proposed fluidic chamber is not used. Insets (a) to (c) present the microscopic images of the area filled with blood and air bubbles with respect to the blood-filled area ϕ_{Blood} [(a) $\phi_{Blood} = 1$, (b) $\phi_{Blood} = 0.5$, and (c) $\phi_{Blood} = 0.2$]. As expected, air bubbles are sequentially delivered into the microfluidic device, which interrupts blood flows in the microfluidic channel. Meanwhile, Fig. 2**C** shows temporal variations of blood volume (V_{Blood}) inside the proposed fluidic chamber and blood-filled area (ϕ_{Blood}) in the ROI of the microfluidic device. Because the fluidic device is sufficiently filled with blood

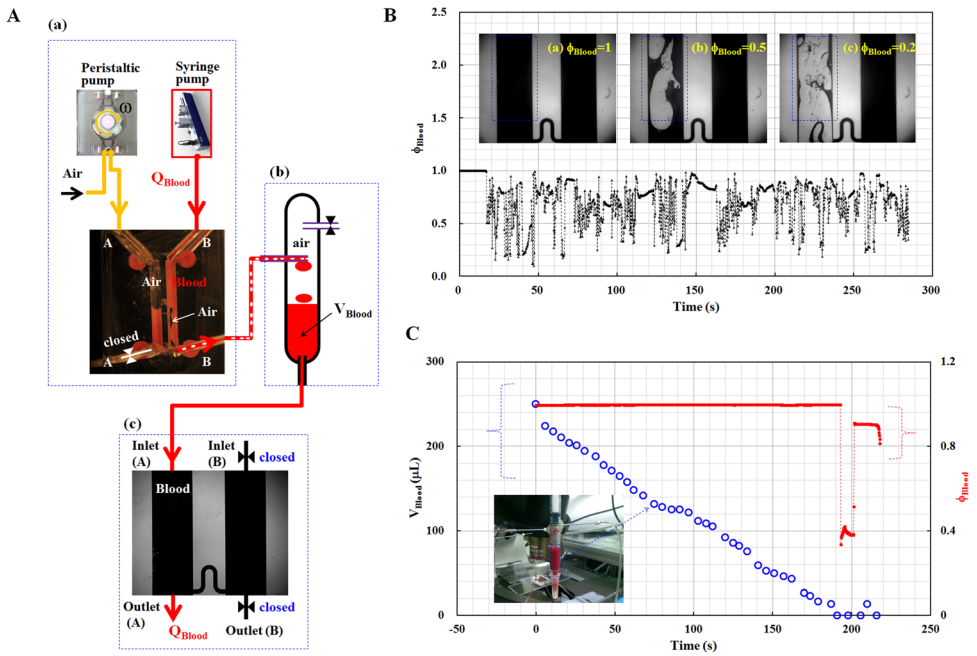

FIG. 2. Quantitative evaluation of bubble-free fluid delivery into a microfluidic device. (**A**) Schematics of experimental setup used to demonstrate bubble-free fluid delivery. The proposed fluidic system is composed of three components; (a) a microfluidic device for test blood with air bubbles, (b) the proposed fluidic chamber for bubble-free delivery, and (c) a microfluidic device for monitoring delivery of air bubbles. After the inlet (B) and the outlet (B) are closed, blood flows in the left- side channel are analyzed using microscopic images captured by a high speed camera. (**B**) Temporal variations of the area filled with blood (ϕ_{Blood}) in a ROI of the left-side channel, without the proposed fluidic device. Insets show microscopic images of the microfluidic channels filled with blood and air bubbles with respect to blood-filled area (ϕ_{Blood}) [(a) $\phi_{Blood} = 1$, (b) $\phi_{Blood} = 0.5$, and (c) $\phi_{Blood} = 0.2$]. (**C**) Temporal variations of the blood volume (V_{Blood}) in the proposed fluidic chamber and the blood-filled area in the ROI in the left-side channel of the microfluidic device.

sample for 191 s, blood is delivered only into the microfluidic device in a bubble-free manner. Thus, the microfluidic channel is filled with pure blood. The blood area remains constant (i.e., $\phi_{Blood} = 1$). Taking into account the fact that air bubbles fill up 0.25 m*l* for 191 s, the flow rate of air bubbles delivered by the peristaltic pump is estimated as 4.71 m*l*/h. However, air bubbles invade into the microfluidic channel, when the blood in the proposed fluidic chamber is empty. The area filled with blood in the ROI (ϕ_{Blood}) is changed, depending on blood volume in the proposed fluidic chamber (V_{liquid}).

These experimental results show that the proposed method can effective supply fluids into the microfluidic device in a bubble-free manner, under the condition of sufficient blood volume in the proposed fluidic chamber.

B. Pulse-free fluid delivery

To demonstrate the pulse-free delivery of the proposed fluidic chamber, pulsatile blood flows were induced by using a peristaltic pump. As shown in Fig. 3**A**, the experimental setup was composed of several components, including a microfluidic device, a proposed fluidic chamber, a peristaltic pump for a pulsatile-flow delivery of blood, a syringe pump for consistent delivery of PBS solution, and a microbalance (AP250D, Ohaus, USA) for flow-rate measurement. Blood (RBCs in PBS suspension, $H_{ct} = 40\%$) was supplied from the reservoir into the proposed fluidic chamber by using the peristaltic pump. Simultaneously, to monitor blood flow in the microfluidic channel, the PBS solution was delivered at a constant flow rate (Q_{PBS}) using the syringe pump. By applying the proposed method, pulsatile flow-rate of blood was stabilized and the test sample was consistently supplied into the inlet (A) of the microfluidic device. The blood-filled width (α_{Blood}) in the right-side channel of the microfluidic channel was evaluated

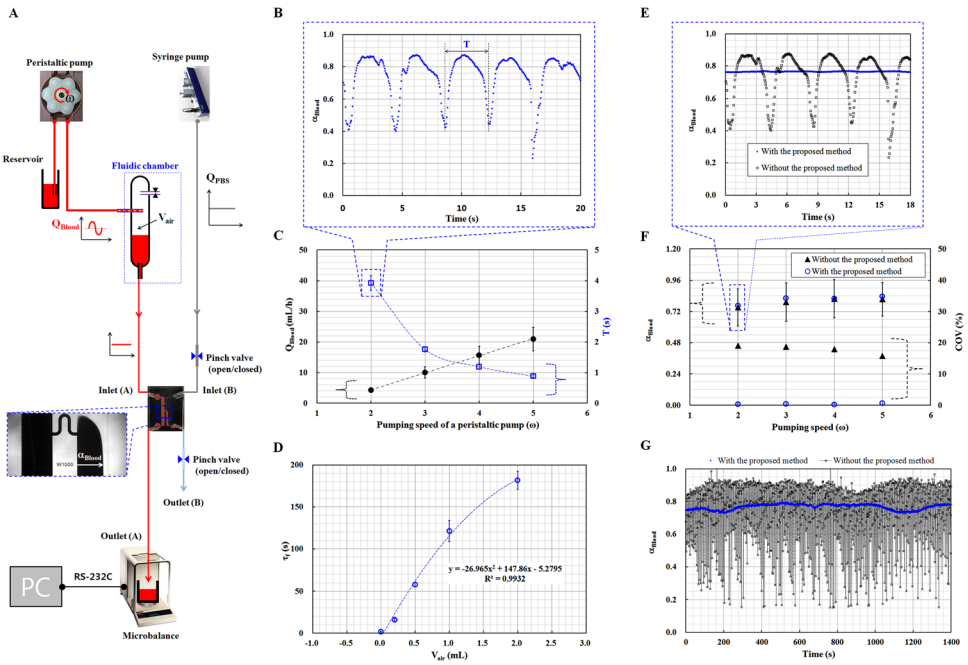

FIG. 3. Quantitative evaluation of the pulse-free fluid delivery based on air compressibility within the proposed fluidic device. (**A**) Schematics of experimental setup used to demonstrate pulse-free fluid delivery. The fluidic system is composed of a microfluidic device, the proposed fluidic chamber, a peristaltic pump for pulsatile delivery of blood, a syringe pump for steady delivery of PBS solution, and a microbalance for flow-rate measurement. (**B**) Temporal variation of the blood-filled width (α_{Blood}) in the right-side channel. The peristaltic pump operates at a pumping speed of 2 ($\omega = 2$), and the syringe pump is set to send PBS solution at a flow rate of 1 m*l*/h ($Q_{PBS} = 1$ m*l*/h). (**C**) Variations of blood flow rate (Q_{Blood}) and the period (T) of the blood-filled width with respect to the pumping speed of the peristaltic pump (ω). (**D**) Variations of time constant (τ_f) with respect to air-filled volume (V_{air}) in the proposed fluidic chamber. (**E**) Quantitative comparison of α_{Blood} without the proposed method ($V_{air} = 0$) and with the proposed method ($V_{air} = 0.5$ m*l*), at the pumping speed of $\omega = 2$. (**F**) Variations of α_{Blood} and COV with respect to the pumping speed (ω). (**G**) Temporal variations of α_{Blood}, with and without the proposed method, at the pumping speed of $\omega = 2$ for 1400 s.

by varying the pumping speed of the pump (ω) and the air-filled volume in the proposed fluidic chamber (V_{air}). After the inlet (B) and the outlet (B) of the microfluidic device were closed, mass variations were measured using a RS-232C communication device positioned between a computer and the microbalance, at a time interval of 1 s. The flow rate of blood (Q_{Blood}) was then calculated using the mass data measured consecutively at time interval (Δt). Q_{Blood} is given as $Q_{Blood} = 1/\rho \cdot \Delta m/\Delta t$. In this study, the parameters ρ and Δm denote the density and mass variation, respectively. To quantify the pulsatile flow-rate of blood delivered by the peristaltic pump, the temporal variations of α_{Blood} were measured under varying pumping speed ranging from 2 to 5 ($\omega = 2$ to 5). To ensure that the interface between blood and PBS solution was located in the right-side channel, the corresponding flow rate of the PBS solution (Q_{PBS}) for each pumping speed (ω) was adjusted as (a) $Q_{PBS} = 1$ m*l*/h for $\omega = 2$, (b) $Q_{PBS} = 1.5$ m*l*/h for $\omega = 3$, (c) $Q_{PBS} = 2$ m*l*/h for $\omega = 4$, and (d) $Q_{PBS} = 2.5$ m*l*/h for $\omega = 5$. As shown in Fig. **3B**, the blood-filled width in the right-side channel (α_{Blood}) was changed periodically, at a pumping speed of 2 ($\omega = 2$).

Fig. **3C** represents the variations of blood flow rate (Q_{Blood}) measured by the microbalance and period (T) of the blood-filled width with varying pumping speed of the peristaltic pump (ω). As a result, the period (T) is decreased significantly from 3.93 ± 0.24 s to 0.88 ± 0.05 s, as pumping speed increases. In addition, the flow rate of blood increases linearly from 4.22 ± 0.77 m*l*/h to 20.98 ± 3.84 m*l*/h, with increasing pumping speed from 2 to 5 (i.e., $\omega = 2$ to 5). To quantify the effect of air-filled volume (V_{air}) on the flow stabilization, a time constant (τ_f) was estimated by measuring change in the flow rate of blood under sudden changes in pumping speed from $\omega = 4$ to $\omega = 0$. As shown in Fig. **3D**, the time constant tends to increase

gradually from 1.62 ± 0.1 s ($V_{air} = 0$) to 181.48 ± 10.79 s ($V_{air} = 2$ m*l*) with increasing air-filled volume (V_{air}) in the proposed fluidic chamber. That is, the flow stabilization effect is enhanced by increasing the air-filled volume in the fluidic chamber. In this test, the air-filled volume is set to 0.5 m*l*, which corresponds to the time constant of 57.83 ± 2.66 s.

Figs. 3E and 3F show the effects of air compressibility on the flow stabilization. In this study, blood was delivered at a pumping speed of 2 ($\omega = 2$). Periodic variations in the blood flow rate were completely removed by employing the proposed fluidic chamber. The blood-filled width (α_{Blood}) remained constant, without respect to the pumping speed (ω). To quantify the effect of the proposed method on flow stabilization, the coefficient of variance (COV) was calculated using the information on blood flow rate. As a result, the COV decreased from 19.1% to 0.2% after the proposed method is applied. In addition, to evaluate the reliability of the proposed method, the blood-filled width (α_{Blood}) was monitored for 1400 s at a time interval of 1 s. As shown in Fig. 3G, by using the proposed method, the blood-filled width remained constant. The COV decreased from 25.5% to 2.3%. Thus, the proposed method can provide bubble-free fluid delivery into the microfluidic device with sufficient reliability. These experimental results lead to a conclusion that the proposed method is capable of delivering fluids into a microfluidic device, with consistency and reliability, even for periodically varying blood flows.

C. Oxygen bubble-free and pulse-free delivery of rat blood

During rat blood perfusion by a peristaltic pump, the pulsatile blood flow contains oxygen bubbles. Thus, the pulsatile flows and oxygen bubbles should be removed to ensure reliable operation of a microfluidic device.[47] As shown in Fig. 4A, to demonstrate the bubble-free and pulse-free delivery of rat blood into the microfluidic device, two proposed fluidic chambers were connected to a complex fluidic network including a rat, a pinch valve, a reservoir, a microfluidic device, a peristaltic pump, and a syringe pump. The cavity volume in the proposed fluidic chamber was set to 0.5 m*l*. The flow rate of the PBS solution was maintained at 3 m*l*/h.

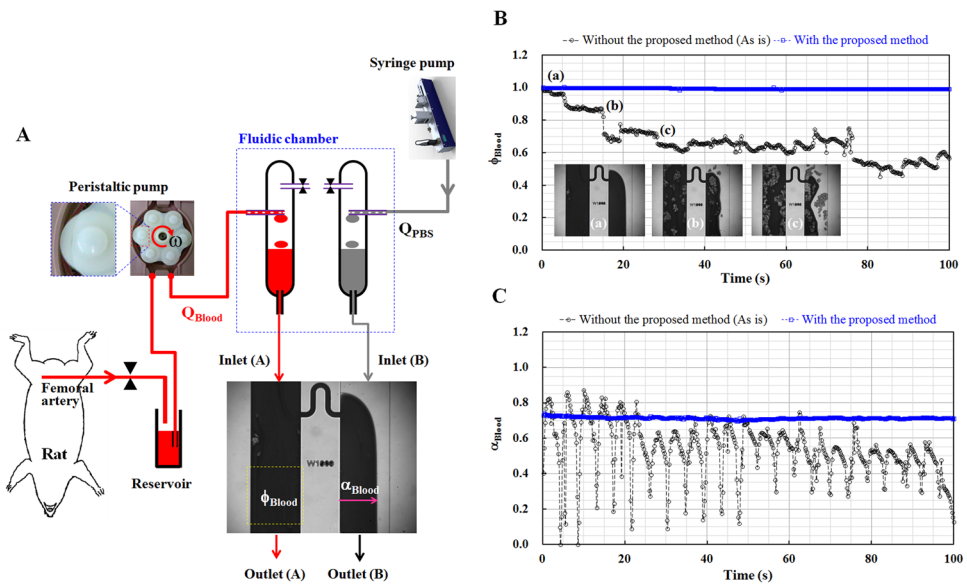

FIG. 4. Performance demonstration of the proposed fluidic device for bubble-free and pulse-free delivery of rat blood into a microfluidic device. (**A**) Schematic diagram for delivering rat blood circulating in a complex fluidic network including a rat, a pinch valve, a reservoir, two proposed fluidic chambers, a microfluidic device, a peristaltic pump, and a syringe pump. The flow rate of PBS solution is maintained at 3 m*l*/h. The peristaltic pump is operated at a pumping speed of $\omega = 2$. Oxygen bubble-free delivery and pulse-free blood-flow are evaluated using the blood-filled area (ϕ_{Blood}) and the blood-filled width (α_{Blood}) in the microfluidic device. (**B**) Comparison of ϕ_{Blood} in the left-side channel, with and without the proposed method. (**C**) Temporal variations of α_{Blood} in the right-side channel, with and without the proposed method.

The peristaltic pump was operated at a pumping speed of $\omega = 2$. The rat blood in the fluidic chamber was filled up to a volume of 0.25 m*l*, by manipulating the pinch valve. The delivery of oxygen bubbles into the microfluidic device was monitored by checking the area filled with blood (ϕ_{Blood}) in a ROI in the left-side channel. In addition, the pulsatile flow rate of rat blood was evaluated using the blood-filled width (α_{Blood}) in the right-side channel.

Fig. 4**B** compares the temporal variations of ϕ_{Blood} in the left-side channel, with and without proposed fluidic chamber. Without the proposed fluidic device, the microfluidic channel was partially filled with oxygen bubbles. Sequentially, the bubbles were migrated along the microfluidic channel. Insets (a) to (c) represent typical microscopic images with respect to blood-filled area (ϕ_{Blood}) [(a) $\phi_{Blood} = 1$, (b) $\phi_{Blood} = 0.85$, and (c) $\phi_{Blood} = 0.72$]. In this demonstration, oxygen bubbles filled up to 40% of specific regions, without the proposed fluidic chamber. However, by applying the proposed fluidic chamber, the blood-filled area (ϕ_{Blood}) remained constant (i.e., $\phi_{Blood} \approx 1$). This result supports that the proposed fluidic chamber is effective for the bubble-free delivery of rat blood. Fig. 4**C** compares the temporal variations of α_{Blood} in the right-side channel, with and without proposed fluidic chamber. Without the proposed fluidic chamber, the blood-filled width (α_{Blood}) unstably varied owing to the operational characteristics of the peristaltic pump and the presence of oxygen bubbles in the microfluidic channels. However, by employing the proposed fluidic device, the blood-filled width remained constant (i.e., $\alpha_{Blood} \approx 0.71$).

These experimental results show that the proposed fluidic chamber is effective in the bubble-free and pulse-free delivery of rat blood, particularly under peristaltic perfusion.

D. Variation in blood flow due to RBCs deformability

To assess the deformability of RBCs based on the temporal variations of blood flow in a microfluidic channel, the two proposed fluidic chambers ($V_{cavity} = 1$ m*l* and $V_{Blood} = 0.25$ m*l*) were employed for the consistent delivery of blood and PBS solution, as shown in Fig. 5**A**. In this study, PBS solution was consistently supplied to monitor blood flow, while interface between two fluids in the upper-side channel of the microfluidic channel was measured. Blood sample and PBS solution were supplied into the inlets (A and B) of a microfluidic device, at the same flow rate ($Q_{PBS} = Q_{Blood}$), using the syringe pump. The microfluidic device was designed to have a side-channel width of 243 μm ($W_s = 243\ \mu$m) and one bridge channel width of 50 μm ($W_b = 50\ \mu$m). By closing the outlet (A), all blood samples injected through the inlet (A) were passed through the narrow bridge channel. These samples then invaded into the upper-side channel. Thus, the upper-side channel was partially filled with blood sample and PBS solution. The blood-filled width (α_{Blood}) in the upper-side channel was used to evaluate the differences in blood flows, depending on the deformability of RBCs in the blood samples.

As shown in Fig. 5**B**, to evaluate the changes in blood flows with respect to blood flow rate ($Q_{Blood} = 1$-7 m*l*/h), variations of blood-filled width (α_{Blood}) were measured for normal human blood (RBCs in PBS suspension, $H_{ct} = 40\%$). The inset of Fig. 5**B** represents the temporal variations of blood-filled width (α_{Blood}) at a flow rate of 3 m*l*/h. The α_{Blood} remains constant (i.e., $\alpha_{Blood}{}^{S} = 0.617 \pm 0.002$), after exhibiting transient behaviors, even under bubble-free and pulse-free conditions. This result implies that RBCs in blood do not interrupt blood flows in the microfluidic channels. The blood-filled width under the steady-state condition ($\alpha_{Blood}{}^{S}$) remains consistent, without respect to blood flow rate ranging from 1 m*l*/h to 7 m*l*/h ($Q_{Blood} = 1$ m*l*/h to 7 m*l*/h). When the blood flow rate exceeds 1 m*l*/h, blood behaves as a Newtonian fluid because the shear rate is considerably higher than 10^3. Under such high shear rate ($\dot{\gamma} > 10^3\ s^{-1}$), the deformability of RBCs has a dominant influence on blood viscosity. Thus, taking into account the fact that blood viscosity is proportional to blood-filled width (i.e., $\mu_{Blood} \sim \alpha_{Blood}$),[48–50] the viscosity ratio of blood in relation to PBS solution is approximately estimated as 1.6 (i.e., $\mu_{Blood}/\mu_{PBS} = 1.6$). This blood viscosity ratio can be used to evaluate the RBC deformability of human blood samples. For convenience, flow rates of blood and PBS solution were fixed at the same flow rate of 1 m*l*/h ($Q_{Blood} = Q_{PBS} = 1$ m*l*/h) in the comparative studies for chemically fixed RBCs and rat bloods. At first, to demonstrate the variations of fluidic flows attributed to

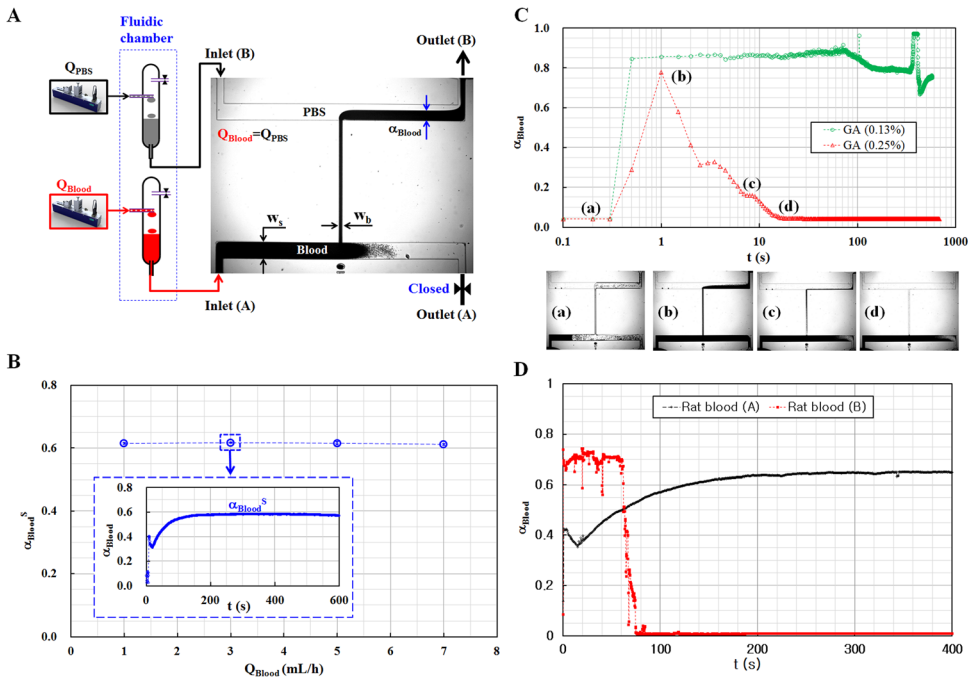

FIG. 5. Evaluation of RBC deformability using temporal variations of blood flows in a microfluidic channel. (**A**) Schematics of experimental setup which is composed of a microfluidic device, two proposed fluidic chambers, and two syringe pumps. The microfluidic device is designed to have side channel width of 243 μm ($W_s = 243\ \mu m$) and bridge channel width of 50 μm ($W_b = 50\ \mu m$). To move all blood samples into the narrow bridge channel, the outlet (A) is closed. (**B**) Variation of blood-filled width (α_{Blood}^S) under steady-state condition with respect to blood flow rate (Q_{Blood}) ($Q_{Blood} = 1$ ml/h to 7 ml/h). Normal blood and PBS solution are delivered at the same flow rate ($Q_{Blood} = Q_{PBS}$). The inset indicates the temporal variations of blood-filled width (α_{Blood}), at the blood flow rate of 3 ml/h. (**C**) Temporal variations of the blood-filled width (α_{Blood}) for blood samples which are chemically hardened by applying two concentrations of GA (0.13% and 0.25%). Microscopic images (a)–(d) show fluidic flows of blood hardened by the GA (0.25%) with respect to time [(a) t = 0.3 s, (b) t = 1 s, (c) t = 7.5 s, and (d) t = 18.5 s]. (**D**) Temporal variations of the blood-filled width (α_{Blood}) for two rat blood samples (A and B).

deformability, blood samples with hardened RBCs (hardened RBCs in PBS suspension, $H_{ct} = 40\%$) were prepared by conducting chemical fixation of normal RBCs using two different concentrations of GA ($C_{GA} = 0.13$ and $C_{GA} = 0.25\%$).

Fig. 5C shows temporal variations of the blood-filled width (α_{Blood}) for two hardened blood samples. The α_{Blood} of the hardened blood sample fixed by the GA (0.13%) was significantly larger than that of normal blood sample. This result indicates that blood viscosity increases with decreasing deformability of RBCs. After 80 s, the value of α_{Blood} becomes unstable, which indicates that the hardened blood might interrupt fluidic flows in the narrow bridge channel. For the hardened blood sample that was chemically fixed by the GA (0.25%), microscopic images (a) to (d) show fluidic flows with respect to time [(a) t = 0.3 s, (b) t = 1 s, (c) t = 7.5 s, and (d) t = 18.5 s]. Due to lower deformability of RBCs, the hardened blood sample was clogged in the bridge channel after 20 s. As the hardened blood sample did not pass through the upper-side channel, the blood volume (V_{Blood}) in the proposed fluidic chamber is increased with respect to time. No blood leakage occurred at the inlet (A), even when blood clogged in the bridge channel. The blood-filled width (α_{Blood}) was then analyzed using two rat blood samples extracted from two rats (A and B). The α_{Blood} of rat blood (A) remained constant after exhibiting transient behavior. The variation trend of α_{Blood} is similar to that of human blood, as shown in Fig. 5B. However, the blood-filled width of the rat blood (B) showed unstable behaviors and decreased to zero after the bridge channel was clogged at $t = 82.2 \pm 26.7$ s ($n = 5$). The deformability of the rat blood A was significantly better than that of rat blood B.

From these experimental results, we conclude that the proposed fluidic chamber can be used to evaluate the changes in deformability of blood samples that pass through narrow microfluidic channel.

E. Variation in blood flows by platelet aggregation

Platelet aggregation usually occurs and adheres on the surfaces, at local positions of high shear-rate ($\dot{\gamma} > 4000\,s^{-1}$).[51] It causes progressive obstruction in blood flows in the local region. To monitor the temporal variations of blood flows caused by platelet aggregation in a microfluidic channel, we established an experimental setup including two proposed fluidic devices ($V_{cavity} = 0.5\,ml$ and $V_{air} = 0.25\,ml$), a microfluidic device, and two syringe pumps, as shown in Fig. 6A. To induce platelet aggregation in the microfluidic channel, rat blood was extracted from a rat. For comparison, the control blood sample without platelets was prepared by removing platelets from the extracted rat blood. The hematocrit of each rat blood sample was carefully adjusted to 40%. To induce high shear rate in the microfluidic channel, a test channel between the inlet (A) and the left-side channel was designed to have 100 μm width ($W_N = 100\,\mu m$). Rat blood and PBS solution were delivered into the inlets (A and B), at the same flow rate of 3 ml/h. The shear rate in the test channel was approximately estimated as $3 \times 10^4\,s^{-1}$ using the wall shear rate formula for a rectangular channel.[48] As the interface between blood and PBS solution was positioned in the right-side channel because blood viscosity was larger than that of PBS solution, the blood-filled width (α_{Blood}) in the right-side channel was employed to monitor the temporal variations of blood flows.

Fig. 6B shows the temporal variations of the blood-filled width (α_{Blood}) for rat blood and rat blood without platelets. The α_{Blood} for rat blood tends to increase over time. Microscopic images (a) to (c) show typical flow patterns of rat blood with respect to time [(a) t = 20 s, (b) t = 60 s, and (c) t = 100 s]. The inset (d) indicates that platelet aggregation is randomly distributed in both channels, after being induced in the test channel. However, the α_{Blood} for rat blood without platelets is remained consistent after transient behaviors. For this case, there is no platelet aggregation in the microfluidic channels, as shown in inset (e) of Fig. 6B.

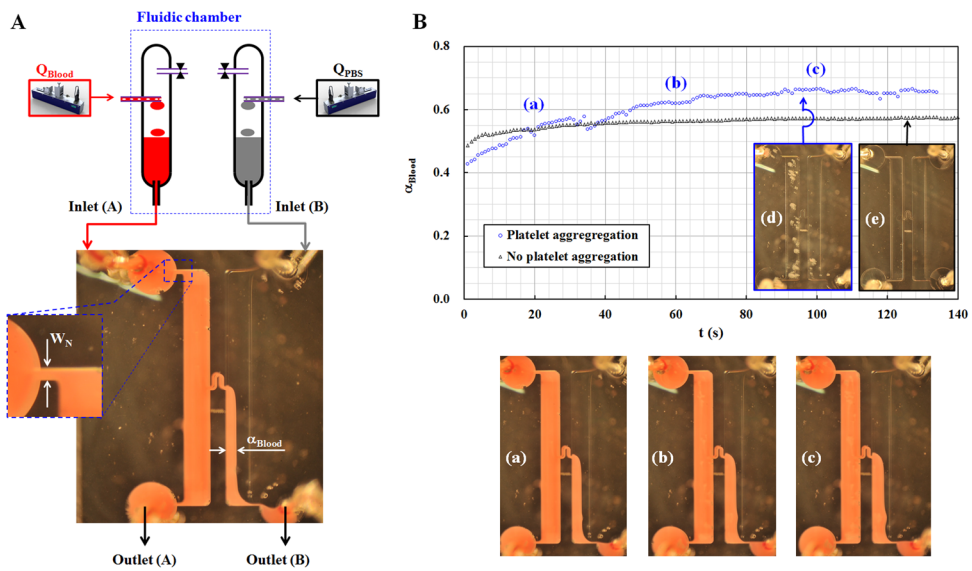

FIG. 6. Quantitative evaluation of platelet aggregation by using temporal variations of fluidic flows in a microfluidic channel. (**A**) Schematics of the experimental setup which is composed of two proposed fluidic chambers, a microfluidic device, and two syringe pumps for supplying blood and PBS solution. (**B**) Temporal variations of the blood-filled width (α_{Blood}) for the rat blood and rat blood without platelets. Microscopic images (a) to (c) show flow patterns of rat blood with respect to time [(a) t = 20 s, (b) t = 60 s, and (c) t = 100 s]. Inset (d) exhibits platelet aggregation of rat blood in the microfluidic channels. However, inset (e) indicates no platelet aggregation in the microfluidic channels when platelets are removed from the rat blood sample.

From this experimental result, we find that the temporal variations of blood-filled width in the right-side channel of the microfluidic device can be used to evaluate the level of platelet aggregation of blood samples.

V. CONCLUSION

In this study, we proposed a new method for the bubble-free and pulse-free fluid delivery into microfluidic devices. By applying the proposed method, gas bubbles were successfully separated from liquids owing to density difference between liquid and gas. In addition, pulsatile flows caused by a peristaltic pump were consistently stabilized by using the air compliance resulting from gas compressibility. To demonstrate the proposed method, we carefully designed a simple, but effective fluidic-chamber composed of two needles for inlet and outlet, one needle for a pinch valve and a specific-sized closed cavity. The pinch valve is served as a fluid controller to fill or supply liquids into a microfluidic device. To demonstrate the usefulness of the proposed fluidic chamber, the performance of bubble-free and pulse-free fluid delivery was evaluated quantitatively. As a result, the proposed method was useful in supplying fluids into the microfluidic device in a bubble-free manner, particularly when sufficient blood volume was preserved in the proposed fluidic chamber. The pulsatile flows caused by a peristaltic pump were consistently stabilized by employing the proposed fluidic chamber. After its feasibility and usefulness were verified, the proposed method was applied to monitor the temporal variations of fluidic flows of rat blood circulating in a complex fluidic network. The experimental results proved that the proposed method is effective for bubble-free and pulse-free delivery of rat blood. In addition, RBC deformability and platelet aggregation could be evaluated using the information on the temporal variation of blood flows in the microfluidic channel. Based on the these experimental results, the proposed method was found to be a promising tool for the effective supply of liquids, including bloods, into a microfluidic device in a bubble-free and pulse-free manner. In the near future, the proposed method will be applied to evaluate the hemorheological properties and hemodynamic properties of blood flows in a rat model with circulatory vascular diseases by using a microfluidic platform.

ACKNOWLEDGMENTS

This work was supported by the National Research Foundation of Korea (NRF) grant funded by the Korea Government (MSIP) (No. 2008-0061991).

[1]A. J. Chung, D. Kimb, and D. Erickson, Lab Chip **8**, 330–338 (2008).
[2]C. P. Foley, N. Nishimura, K. B. Neeves, C. B. Schaffer, and W. L. Olbricht, Biomed. Microdevices **11**, 915–924 (2009).
[3]N. M. Elman, H. L. H. Duc, and M. J. Cima, Biomed. Microdevices **11**, 625–631 (2009).
[4]B. Cordovez, A. J. Chung, M. Mak, and D. Erickson, Microfluid. Nanofluid. **10**, 785–791 (2011).
[5]C. Dammann, B. Noding, and S. Kostera, Biomicrofluidics **6**, 022009 (2012).
[6]P. Woias, Sens. Actuator, B **105**, 28–38 (2004).
[7]A. Nilghaz, D. H. B. Wicaksono, D. Gustiono, F. A. A. Majid, E. Supriyanto, and M. R. A. Kadir, Lab Chip **12**, 209–218 (2012).
[8]T. Songjaroen, W. Dungchai, O. Chailapakul, C. S. Henry, and W. Laiwattanapaisal, Lab Chip **12**, 3393–3398 (2012).
[9]S. Demming, G. Peterat, A. Llobera, H. Schmolke, A. Bruns, M. Kohlstedt, A. Al-Halhouli, C.-P. Klages, R. Krull, and S. Büttgenbach, Biomicrofluidics **6**, 034106 (2012).
[10]T. H. Schulte, R. L. Bardell, and B. H. Weigl, Clin. Chim. Acta **321**, 1–10 (2002).
[11]A. E. Herr, A. V. Hatch, D. J. Throckmorton, H. M. Tran, J. S. Brennan, W. V. Giannobile, and A. K. Singh, Proc. Natl. Acad. Sci. U.S.A. **104**, 5268–5273 (2007).
[12]V. Srinivasan, V. K. Pamula, and R. B. Fair, Lab Chip **4**, 310–315 (2004).
[13]P. Yager, T. Edwards, E. Fu, K. Helton, K. Nelson, M. R. Tam, and B. H. Weigl, Nature **442**, 412–418 (2006).
[14]S. Sia and L. Kricka, Lab Chip **8**, 1982–1983 (2008).
[15]S. Moon, H. O. Keles, A. Ozcan, A. Khademhosseini, E. Hæggstrom, D. Kuritzkes, and U. Demirci, Biosens. Bioelectron. **24**, 3208–3214 (2009).
[16]J. Li and F. Lin, Trends Cell Biol. **21**, 489–497 (2011).
[17]S.-Y. Cheng, S. Heilman, M. Wasserman, S. Archer, M. L. Shuler, and M. Wu, Lab Chip **7**, 763–769 (2007).
[18]P. Preira, M.-P. Valignat, J. Bico, and O. Theodoly, Biomicrofluidics **7**, 024111 (2013).
[19]C. Yi, C.-W. Li, S. Ji, and M. Yang, Anal. Chim. Acta **560**, 1–23 (2006).
[20]W. Hellmich, C. Pelargus, K. Leffhalm, A. Ros, and D. Anselmetti, Electrophoresis **26**, 3689–3696 (2005).
[21]N. Vertti-Quintero, Y. Song, P. Manneville, and C. N. Baroud, Biomicrofluidics **6**, 034105 (2012).
[22]S. S. Bithi and S. A. Vanapalli, Biomicrofluidics **4**, 044110 (2010).

[23]C.-Y. Lee, C.-L. Chang, Y.-N. Wang, and L.-M. Fu, Int. J. Mol. Sci. **12**, 3263–3287 (2011).
[24]P. Garstecki, M. J. Fuerstman, M. A. Fischbach, S. K. Sia, and G. M. Whitesides, Lab Chip **6**, 207–212 (2006).
[25]H. Y. Park, X. Qiu, E. Rhoades, J. Korlach, L. W. Kwok, W. R. Zipfel, W. W. Webb, and L. Pollack, Anal. Chem. **78**, 4465–4473 (2006).
[26]L. Y. Yeo, H.-C. Chang, P. P. Y. Chan, and J. R. Friend, Small **7**, 12–48 (2011).
[27]A. R. Abate and D. A. Weitz, Biomicrofluidics **5**, 014107 (2011).
[28]H. M. Wyss, D. L. Blair, J. F. Morris, H. A. Stone, and D. A. Weitz, Phys. Rev. E **74**, 061402 (2006).
[29]S.-B. Huang, Y. Zhaob, D. Chen, H.-C. Lee, Y. Luo, T.-K. Chiu, J. Wang, J. Chen, and M.-H. Wu, Sens. Actuator, B **190**, 928–936 (2014).
[30]B.-h. Chueh, D. Huh, C. R. Kyrtsos, T. Houssin, N. Futai, and S. Takayama, Anal. Chem. **79**, 3504–3508 (2007).
[31]W. Zheng, Z. Wang, W. Zhang, and X. Jiang, Lab Chip **10**, 2906–2910 (2010).
[32]B. Yang and Q. Lin, J. Microelectromech. Syst. **18**, 539–546 (2009).
[33]Y. Zheng, J. Nguyen, Y. Wei, and Y. Sun, Lab Chip **13**, 2464–2483 (2013).
[34]Z. Yang, S. Matsumoto, and R. Maeda, Sens. Actuator, A **95**, 274–280 (2002).
[35]E. Kang, D. H. Lee, C.-B. Kim, S. J. Yoo, and S.-H. Lee, J. Micromech. Microeng. **20**, 045009 (2010).
[36]J. H. Sung and M. L. Shuler, Biomed. Microdevices **11**, 731–738 (2009).
[37]C. Lochovsky, S. Yasotharan, and A. Gunther, Lab Chip **12**, 595–601 (2012).
[38]A. M. Skelley and J. Voldman, Lab Chip **8**, 1733–1737 (2008).
[39]J. Xu, R. Vaillant, and D. Attinger, Microfluid. Nanofluid. **9**, 765–772 (2010).
[40]C. Liu, J. A. Thompson, and H. H. Bau, Lab Chip **11**, 1688–1693 (2011).
[41]J. M. Karlsson, M. Gazin, S. Laakso, T. Haraldsson, S. Malhotra-Kumar, M. Mäki, H. Goossensb, and W. van der Wijngaarta, Lab Chip **13**, 4366–4373 (2013).
[42]M. Johnson, G. Liddiard, M. Eddings, and B. Gale, J. Micromech. Microeng. **19**, 095011 (2009).
[43]I. Doh and Y.-H. Cho, Lab Chip **9**, 2070–2075 (2009).
[44]Y. J. Kang and S. Yang, Lab Chip **12**, 1881–1889 (2012).
[45]D. C. Leslie, C. J. Easley, E. Seker, J. M. Karlinsey, M. Utz, M. R. Begley, and J. P. Landers, Nat. Phys. **5**, 231–235 (2009).
[46]B. Mosadegh, C.-H. Kuo, Y.-C. Tung, Y.-s. Torisawa, T. Bersano-Begey, H. Tavana, and S. Takayama, Nat. Phys. **6**, 433–437 (2010).
[47]Y. J. Kang, E. Yeom, and S.-J. Lee, Anal. Chem. **85**, 10503–10511 (2013).
[48]Y. J. Kang, J. Ryu, and S.-J. Lee, Biomicrofluidics **7**, 044106 (2013).
[49]Y. J. Kang and S.-J. Lee, Biomicrofluidics **7**, 054122 (2013).
[50]Y. J. Kang, E. Yeom, and S.-J. Lee, Biomicrofluidics **7**, 054111 (2013).
[51]M. Li, D. N. Ku, and C. R. Forest, Lab Chip **12**, 1355–1362 (2012).